

RESEARCH ARTICLE | MAY 16 2023

## CNT effective interfacial energy and pre-exponential kinetic factor from measured NaCl crystal nucleation time distributions in contracting microdroplets



Ruel Cedeno; Romain Grossier ; Nadine Candoni; ... et. al



*J. Chem. Phys.* 158, 194705 (2023)

<https://doi.org/10.1063/5.0143704>



CrossMark

Time to get excited.  
Lock-in Amplifiers – from DC to 8.5 GHz

[Find out more](#)

Zurich Instruments

# CNT effective interfacial energy and pre-exponential kinetic factor from measured NaCl crystal nucleation time distributions in contracting microdroplets



Cite as: J. Chem. Phys. 158, 194705 (2023); doi: 10.1063/5.0143704

Submitted: 25 January 2023 • Accepted: 29 March 2023 •

Published Online: 16 May 2023




View Online



Export Citation



CrossMark

Ruel Cedeno,<sup>1,2</sup>  Romain Grossier,<sup>1,a)</sup>  Nadine Candoni,<sup>1</sup>  Nicolas Levernier,<sup>3,4</sup> Adrian E. Flood,<sup>2,a)</sup>   
and Stéphane Veesler<sup>1,a)</sup> 

## AFFILIATIONS

<sup>1</sup> CNRS, Aix-Marseille University, CINaM (Centre Interdisciplinaire de Nanosciences de Marseille), Campus de Luminy, Case 913, F-13288 Marseille Cedex 09, France

<sup>2</sup> Department of Chemical and Biomolecular Engineering, School of Energy Science and Engineering, Vidyasirimedhi Institute of Science and Technology, Rayong 21210, Thailand

<sup>3</sup> INMED, INSERM, Aix Marseille University, Turing Centre for Living Systems, Marseille, France

<sup>4</sup> Aix-Marseille University, Université de Toulon, CNRS, CPT (UMR 7332), Turing Centre for Living Systems, Marseille, France

**Note:** This paper is part of the JCP Special Topic on Nucleation: Current Understanding Approaching 150 Years After Gibbs.

**a) Authors to whom correspondence should be addressed:** [romain.grossier@cnrs.fr](mailto:romain.grossier@cnrs.fr); [adrian.flood@vistec.ac.th](mailto:adrian.flood@vistec.ac.th); and [stephane.veesler@cnrs.fr](mailto:stephane.veesler@cnrs.fr)

## ABSTRACT

Nucleation, the birth of a stable cluster from a disorder, is inherently stochastic. Yet up to date, there are no quantitative studies on NaCl nucleation that accounts for its stochastic nature. Here, we report the first stochastic treatment of NaCl-water nucleation kinetics. Using a recently developed microfluidic system and evaporation model, our measured interfacial energies extracted from a modified Poisson distribution of nucleation time show an excellent agreement with theoretical predictions. Furthermore, analysis of nucleation parameters in 0.5, 1.5, and 5.5 pl microdroplets reveals an interesting interplay between confinement effects and shifting of nucleation mechanisms. Overall, our findings highlight the need to treat nucleation stochastically rather than deterministically to bridge the gap between theory and experiment.

Published under an exclusive license by AIP Publishing. <https://doi.org/10.1063/5.0143704>

## I. INTRODUCTION

Nucleation plays a key role in a wide array of applications, including nano-synthesis,<sup>1</sup> energy storage,<sup>2</sup> pharmaceutical production, biomineralization, and climate modeling.<sup>3</sup> Sodium chloride, being the most abundant salt on Earth,<sup>4</sup> is of particular interest due to its influence on metal corrosion,<sup>5</sup> building material degradation,<sup>6</sup> oil well productivity,<sup>7</sup> atmospheric science,<sup>3</sup> and so on. Thus, a fundamental understanding of its nucleation kinetics is of paramount importance, yet it remains poorly understood from both experimental and theoretical perspectives.<sup>8</sup> Indeed, nucleation rates from simulations still differ from experiments by several orders of magnitude.<sup>8,9</sup> With diverse simulation approaches

being applied,<sup>8,10–14</sup> reliable benchmarking of computational results with experiments remains a challenge as there are only very few experimental studies that quantitatively measure the nucleation kinetic parameters of NaCl in water. These include experiments that employ an efflorescence chamber,<sup>15</sup> an electrodynamic levitator,<sup>16</sup> and microcapillaries,<sup>4</sup> all of which treated nucleation deterministically. In this context, deterministic methods calculate nucleation rates directly from the mean nucleation time, whereas stochastic methods employ the probability distribution of nucleation times. However, primary nucleation has been shown to be inherently stochastic rather than deterministic.<sup>17,18</sup> Moreover, because nucleation is a rare event and the critical nucleus is a transient species, it is barely undetectable by classical experiments. This can

be addressed by introducing a local bias in the solution so that nucleation is much more probable.<sup>19</sup> Recently, with *in situ* electron microscopy, Nakamura *et al.*<sup>20</sup> captured the atomically resolved images of NaCl nucleation in confined conical carbon nanotubes (with volume confinement as a bias). They observed that a critical cluster must have at least 48 NaCl units and that the nucleation periods follow a normal distribution spanning from 2 to 10 s based on nine nucleation events. Although more data points are needed to generate a reliable statistical distribution, this is a piece of strong evidence for the stochasticity of NaCl nucleation, yet surprisingly, there are no existing experimental studies that measure its kinetic parameters using the stochastic view of nucleation. In this article, we address this by measuring the primary nucleation kinetic parameters of aqueous NaCl in confined microdroplets, in the pl range, with a stochastic model. We demonstrate that by combining the deliquescence–recrystallization cycle for measuring induction times,<sup>21</sup> an appropriate evaporation model,<sup>22</sup> together with an inhomogeneous Poisson probability distribution of nucleation time,<sup>23</sup> and the Classical Nucleation Theory (CNT), one can obtain a reliable estimate of nucleation parameters, effective interfacial energy<sup>24</sup> and pre-exponential kinetic factor, which are consistent with theoretical and experimental values from the literature. Finally, we analyze the impact of confinement by volume<sup>25,26</sup> on the measured kinetic parameters.

## II. MATERIALS AND METHODS

Arrays of sessile NaCl microdroplets are generated on PMMA-coated glass immersed in a thin layer of polydimethylsiloxane (PDMS) oil at ambient conditions (1 atm, 25 °C). Supersaturation

to achieve nucleation is obtained via the droplet contraction technique<sup>27</sup> (similar to an evaporation process) under controlled humidity (10% RH) using the method described in our previous work.<sup>21</sup> A schematic overview of the setup and illustration of the droplet contraction technique is shown in Figs. 1(a) and 1(b), while selected microdroplet images are shown in Figs. 1(c) and 1(d).

For each droplet, we calculate the dimensionless nucleation time<sup>21</sup>  $\tau$ , i.e., the time elapsed between saturation and the nucleation point divided by a characteristic time accounting for the evaporation rate.<sup>21</sup> This is a pre-processing procedure to robustly take into account the variability of the evaporation rate in the setup.<sup>28</sup> We also verified that there is no interference of diffusion-mediated interactions between microdroplets.<sup>21</sup> To find the volume and supersaturation ratio as a function of  $\tau$ , we employed an evaporation model tailored to our specific configuration.<sup>22</sup> We then plot the cumulative probability distribution of supersaturation ratio at nucleation (i.e., the fraction of the microdroplets that has nucleated at a given supersaturation ratio) for each set of microdroplet sizes. We then fit the distribution of nucleation times with the help of an inhomogeneous Poisson distribution, as proposed by Goh *et al.*,<sup>23</sup> under conditions of time-varying supersaturation,

$$P(t) = 1 - \exp\left[-\int_{t_{\text{sat}}}^{t_{\text{nuc}}} J(t)V(t)dt\right], \quad (1)$$

with  $P(t)$  being the fraction of microdroplets nucleated after time  $t$ ,  $V(t)$  being the droplet volume at time  $t$ ,  $t_{\text{sat}}$  being the time at which the microdroplet becomes saturated, and  $t_{\text{nuc}}$  being the nucleation time.

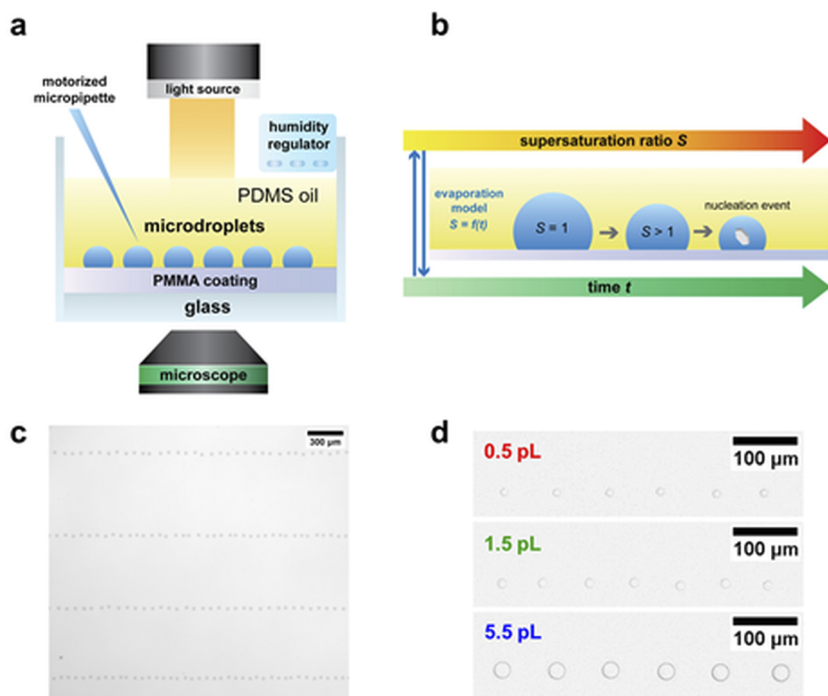


FIG. 1. (a) Schematic overview of the experimental setup (adapted from Ref. 22), (b) illustration of droplet evaporation until nucleation, (c) image of a typical 2D array of microdroplets, and (d) image of microdroplets at saturation across different sizes at saturation.

For the primary nucleation rate  $J(t)$ , we used the classical nucleation theory (CNT) as

$$J(t) = A \exp \left[ -\frac{16\pi}{3} \frac{\gamma_{\text{eff}}^3}{\rho_s^2 (k_b T)^3 \ln^2 \left( \frac{\gamma_{\pm} S(t)}{\gamma_{\pm 0}} \right)} \right], \quad (2)$$

where  $A$  is the pre-exponential factor,  $\gamma_{\text{eff}}$  is the effective interfacial energy,  $\rho_s$  is the number density of formula units in the solid ( $2.27 \times 10^{28} \text{ m}^{-3}$  for NaCl),  $k_b T$  is the thermal energy,  $S(t)$  is the supersaturation expressed as the ratio of concentrations (concentration at nucleation/concentration at saturation) at nucleation at time  $t$ , and  $\gamma_{\pm}$  and  $\gamma_{\pm 0}$  are the ionic activities at  $S(t)$  and at saturation, respectively (see Secs. S1–S3 of the supplementary material). This represents a general equation for primary nucleation with  $\gamma_{\text{eff}}$  accounting for the “degree” of heterogeneity. While analytical solutions for Eqs. (1) and (2) exist for special cases,<sup>29</sup> our evolution of supersaturation ratio  $S(t)$  with time is governed by a system-specific evaporation model<sup>22</sup> (see Sec. S4 of the supplementary material) whose complexity requires a numerical approach (see Sec. S5 of the supplementary material).

Furthermore, thanks to the small droplet size coupled with hindered evaporation rate (due to the oil layer), diffusion dominates over convection (Peclet number  $< 10^{-3}$ , see Sec. S4.3 of the supplementary material). As a result, the microdroplets maintain a uniform concentration distribution,<sup>22</sup> instead of being concentrated at the interface or contact line (in contrast to  $\mu\text{l}$  droplets directly evaporating in the air).<sup>30</sup>

### III. RESULTS AND DISCUSSION

With the nucleation times obtained via image analysis, we computed the normalized nucleation time  $\tau$ , and the results are plotted in Fig. 2(a). Using our tailored evaporation model,  $\tau$  can then be converted into distributions of supersaturation ratios at nucleation, as shown in Fig. 2(b). As shown in Fig. 2(b), the combination of the inhomogeneous Poisson distribution [Eq. (1)] and classical nucleation theory [Eq. (2)] well captures the sigmoidal nature of the distribution. Unlike the use of empirical distributions (such as Weibull, Gompertz, and Gumbel, whose parameters cannot be interpreted in terms of CNT, this method allows the extraction of the kinetic parameter  $A$  (pre-exponential factor) and

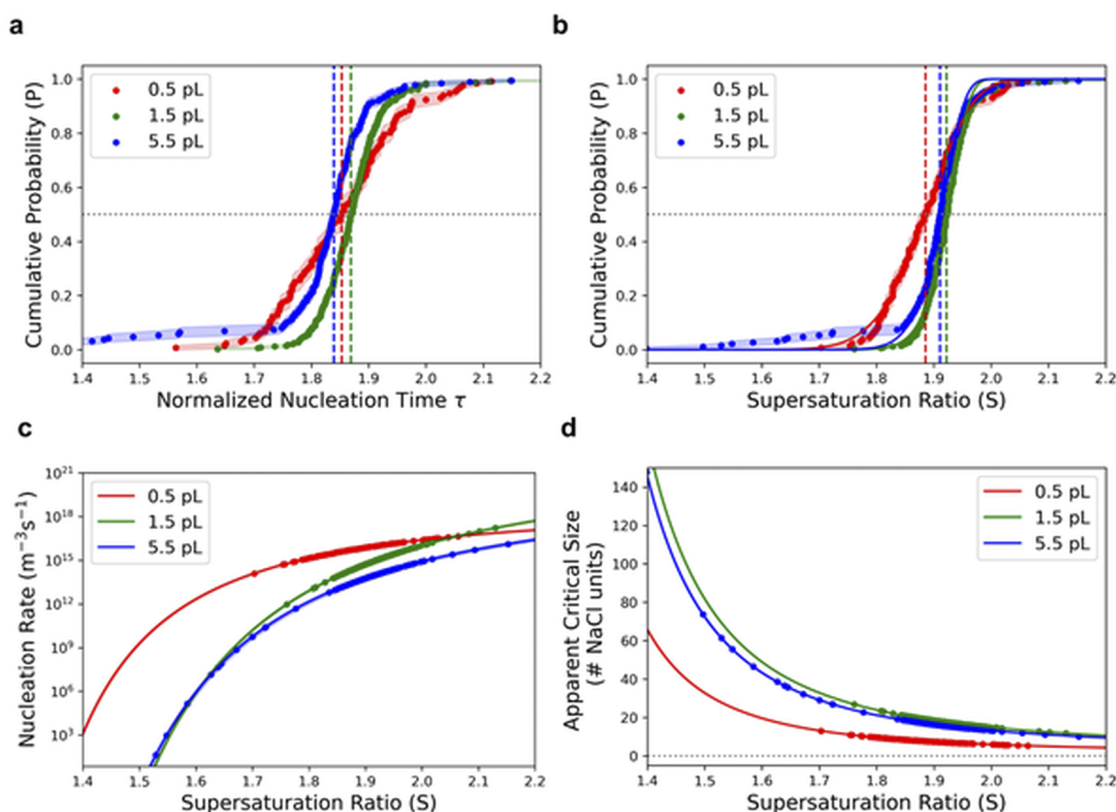


**FIG. 2.** (a) Cumulative distribution of normalized nucleation time  $\tau$  for 0.5 pL ( $N = 131$ ), 1.5 pL ( $N = 337$ ), and 5.5 pL ( $N = 187$ ) and their corresponding error bands. The median  $\tau$  is marked by dashed vertical lines, and  $P = 0.5$  is marked by the gray dotted line. (b) Fitting of the inhomogeneous Poisson distribution [Eq. (1)] with the experimental distribution of supersaturation ratio at nucleation. The median  $S$  is marked by dashed vertical lines. (c) Nucleation rate ( $J$  in  $\text{m}^{-3} \text{s}^{-1}$ ) as a function of supersaturation ratio computed using the kinetic parameters in Table I. (d) Apparent critical size (No. of NaCl units) as a function of supersaturation ratio computed using the fitted effective interfacial energy  $\gamma_{\text{eff}}$ .

thermodynamic parameter  $\gamma_{\text{eff}}$  (effective interfacial energy between crystal and solution). In theory,  $\gamma_{\text{eff}}$  reflects how the thermodynamic barrier is reduced due to heterogeneous nucleation, that is, if  $\gamma_{\text{HOM}}$  is the homogeneous interfacial energy, then  $\gamma_{\text{eff}}$  lies within  $0 < \gamma_{\text{eff}} < \gamma_{\text{HOM}}$ . The fitted nucleation parameters are listed in Table I. These parameters can then be used to calculate the nucleation rate  $J$  and apparent critical size  $n^*$  as a function of supersaturation ratio  $S$ , which are shown in Figs. 2(c) and 2(d), respectively. Note that the apparent critical size  $n^*$  is calculated based on an equivalent spherical nucleus with an interfacial energy of  $\gamma_{\text{eff}}$ . This is an approximation to the actual critical size, which theoretically depends on the contact angle between the nucleus and the substrate<sup>24</sup> as well as the shape factor of the nucleus.<sup>31</sup> Moreover, since  $n^*$  is calculated based on  $\gamma_{\text{eff}}$ , it also takes into account the effect of heterogeneous nucleation.

To explain the observed trends with respect to volume in Fig. 2 and Table I, we consider two relevant phenomena: (1) the interplay between homogeneous and heterogeneous mechanisms and (2) confinement effects (kinetic and thermodynamic).

Although the median supersaturation  $\bar{S}_n$  is essentially identical for the three studied volumes, the effective interfacial energy  $\gamma_{\text{eff}}$  of the 0.5 pl set is significantly lower than that of the rest. Note that a lower effective thermodynamic barrier is characteristic of the heterogeneous nucleation mechanism. As smaller droplets have a higher surface area to volume ratio, the probability of surface nucleation becomes more apparent relative to bulk nucleation. Moreover, lower supersaturation generally favors the heterogeneous mechanism, while higher supersaturation  $S$  generally favors homogeneous nucleation. This is consistent with the plot of nucleation rate  $J$  against supersaturation ratio [Fig. 2(c)] where we see that at lower  $S$ , the smallest droplet size nucleates faster. However, if the process is governed entirely by the interplay between heterogeneous and homogeneous mechanisms, then we would expect that the thermodynamic barrier  $\gamma_{\text{eff}}$  should obey  $0.5 \text{ pl} < 1.5 \text{ pl} < 5.5 \text{ pl}$ . Interestingly, what we observe for  $\gamma_{\text{eff}}$  is  $0.5 \text{ pl} < 5.5 \text{ pl} \leq 1.5 \text{ pl}$ . This suggests that other phenomena must be at play. Since the droplet volume is in the picoliter range, kinetic and thermodynamical confinements could have an impact. Note that kinetic confinement stems from the fact that nucleation time scales inversely with the nucleation rate  $J$  and system volume  $V$ , i.e.,  $t_n \propto \frac{1}{JV}$ . On the other hand, thermodynamic confinement originates from the depletion of the effective supersaturation<sup>26</sup> level during the formation of the pre-critical clusters in a finite-sized system. In such finite systems, the critical size is determined at a lower “effective” supersaturation, so the critical size would be larger than that of an infinite

system where no depletion occurs. In other words, translated in an infinite system where such confinement through depletion is not taken into account (as in the proposed model herein), it would correspond to a (virtually) higher effective surface energy  $\gamma_{\text{eff}}$ . However, the exact quantification of such thermodynamic confinement through depletion effects as sub-critical population emerge in solution is difficult. This would necessitate, at least, the exact knowledge of the distribution of pre-critical clusters. Nevertheless, we could get some trends from previous works: the higher the solute solubility, the lesser the impact of thermodynamic confinement. For instance, if one compares NaCl and AgCl (known for its low solubility in water) using a “toy model,”<sup>26</sup> we see that the depletion effects in supersaturation needed to form a single critical cluster have a minor role in the case of NaCl but a dramatic effect in the case of AgCl (as shown in Fig. S5 of the supplementary material). This could explain the slight increase in  $\gamma_{\text{eff}}$  as the volume decreases from 5.5 to 1.5 pl. In other words, the observed trend in  $\gamma_{\text{eff}}$  could originate from the competition between heterogeneous nucleation and confinement effects, i.e., heterogeneous nucleation tends to decrease  $\gamma_{\text{eff}}$ , while confinement tends to increase  $\gamma_{\text{eff}}$ . Specific experiments to address this particular problem would need to be made, with a larger range in addressed droplet volumes and comparison with salts/molecules of diverse solubilities. Regarding the kinetic prefactor, its interpretation is generally more complex as it is related to the mass transfer rate of the monomers to the cluster surface, which is a function of the attachment–detachment frequency, viscosity, diffusivity, Zeldovich factor, the concentration of nucleation sites, etc.

Nevertheless, we remind the reader that the analysis presented here is based on the classical nucleation theory (CNT), which has been shown to have inherent limitations, particularly at high supersaturations. In such conditions, the critical size shrinks to dramatically small sizes where the discontinuity of matter (atoms) should play a role or, at least, be the source of large deviations from a CNT set of hypothesis (in particular, the capillary approximation<sup>32</sup>). Although non-classical nucleation theories have been developed,<sup>33,34</sup> their governing equations are more complex and contain multiple fitting parameters. For this reason, we chose CNT to model our experimental data. Moreover, using CNT would allow us to compare our results against the literature (both experiments and simulations). For instance, our fitted  $\gamma_{\text{eff}}$  ranges from 47.5 to 64.5 mJ/m<sup>2</sup> (Table I). These values are consistent with that of Hwang *et al.*<sup>35</sup> who reported  $\gamma_{\text{eff}} = 46.17 \text{ mJ/m}^2$  via an electrostatic levitation experiment. Interestingly, a seeded atomistic simulation performed by the group of Zimmermann *et al.*<sup>10</sup> resulted in an interfacial energy of  $\gamma = 47 \text{ mJ/m}^2$ , while the molecular dynamics simulation of Bahadur *et al.*<sup>12</sup> yielded a  $\gamma$  of 63 mJ/m. This is a reasonable agreement between theory and experiment.

For further comparison with the literature, we then plotted the nucleation rate  $J$  as a function of supersaturation ratio  $S$  in Fig. 3 together with the experimental and simulated data from multiple research groups. We can see that the magnitude of our measured nucleation rate is very close to that of Gao *et al.*<sup>15</sup> measured in an effluorescence chamber experiment and Na. *et al.*<sup>16</sup> who used an electrodynamic levitator trap, a setup that aimed to minimize all possible heterogeneous nucleation sites. Although they reported an interfacial energy between crystal and solution  $\gamma = 87 \text{ mJ/m}^2$ , they calculated it from the average induction time

**TABLE I.** Nucleation kinetic parameters and their corresponding standard error obtained from the fit in Fig. 2(b).

Volume at saturation $V_{\text{sat}}$ (pL)	Median $S$ at nucleation, $\bar{S}_n$	Effective interfacial energy $\gamma_{\text{eff}}$ (mJ/m <sup>2</sup> )	Kinetic prefactor $\log_{10} A$ (m <sup>-3</sup> s <sup>-1</sup> )
0.5	1.89 ( $\pm 3\%$ )	47.5 ( $\pm 0.4\%$ )	19.8 ( $\pm 0.2\%$ )
1.5	1.92 ( $\pm 3\%$ )	64.5 ( $\pm 0.2\%$ )	24.4 ( $\pm 0.3\%$ )
5.5	1.91 ( $\pm 5\%$ )	61.9 ( $\pm 0.4\%$ )	22.3 ( $\pm 0.5\%$ )

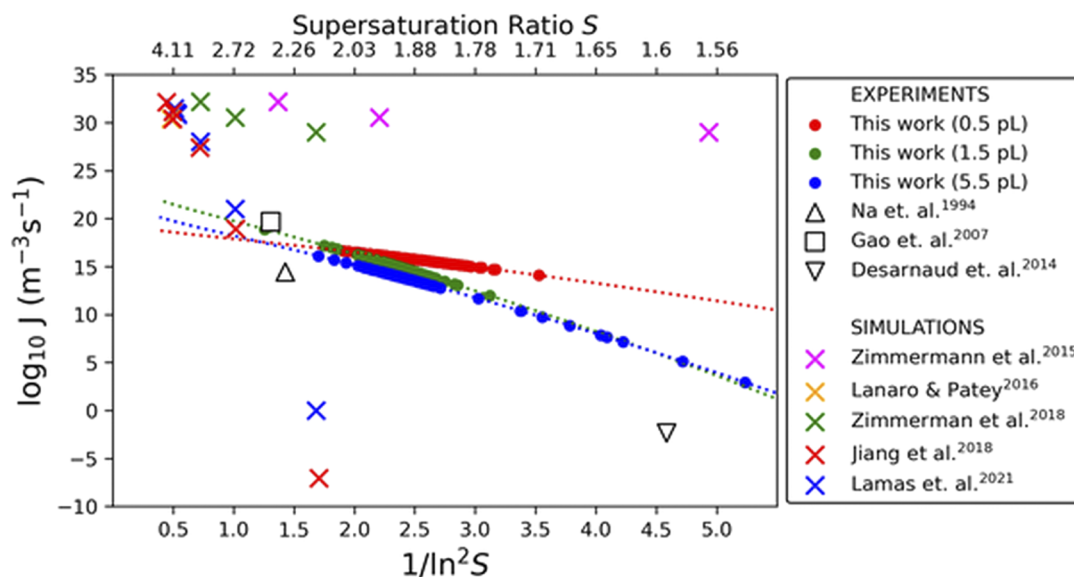


**FIG. 3.** Linearized CNT plot containing the nucleation rate (expressed as  $\log_{10} J$ ) of NaCl in water as a function of supersaturation ( $1/\ln^2 S$  and  $S$  for the bottom and top axis, respectively). Comparison of our experimental results (the dashed blue line is via the extrapolation of CNT) to relevant experimental literature data and theoretical simulations. Experiments were based on an efflorescence chamber (Gao *et al.*,<sup>15</sup> a spherical void electrodynamic levitator trap (Na. *et al.*,<sup>16</sup> and microcapillaries (Desarnaud *et al.*,<sup>4</sup> while the simulations were based on seeded atomistic simulations (Zimmerman *et al.*,<sup>8,10</sup> forward flux sampling (Jiang *et al.*,<sup>14</sup> direct molecular dynamics (Lanaro and Patey),<sup>13</sup> and seeding simulations (Lamas *et al.*,<sup>36</sup>

while taking  $A = 10^{30} \text{ m}^{-3} \text{ s}^{-1}$  as a fixed value (taking induction time as deterministic rather than stochastic). Interestingly, when we used a similar calculation procedure (average induction time and  $A = 10^{30} \text{ m}^{-3} \text{ s}^{-1}$ ), we obtained a value of effective interfacial energy  $\gamma_{\text{eff}}$  of 77, 79, and 80  $\text{mJ/m}^2$  for 0.5, 1.5, and 5.5  $\mu\text{l}$ , respectively (while the stochastic approach yields 47.5, 64.5, and 61.9  $\text{mJ/m}^2$  as shown in Table I, which are closer to the simulation results in the literature).

Thus, the discrepancy in the measured interfacial energy is likely due to two main reasons. First, their approach assumes nucleation as a deterministic process (based on average induction time), while our treatment considers its inherent probabilistic nature (a more realistic view of nucleation). Second, we did not assume any pre-defined value of the pre-exponential factor in the parameter estimation. In the experimental work of Gao *et al.*<sup>15</sup> where they measured mean efflorescence time, they also fixed the prefactor at a value of  $2.8 \times 10^{38} \text{ m}^{-3} \text{ s}^{-1}$ . Furthermore, in the microcapillary experiments of Desarnaud *et al.*,<sup>4</sup> they reported  $J = 0.004 \text{ m}^{-3} \text{ s}^{-1}$  at  $S \approx 1.6$ , but they fixed the value of  $\gamma$  at 80  $\text{mJ/m}^2$ . While there are other experimental studies on NaCl–water nucleation,<sup>30,35,37,38</sup> values of either nucleation rates or driving forces were not explicitly reported, so we are unable to include them in Fig. 3. Thus, to the best of our knowledge, our work is the first experimental work that employed a probabilistic approach to measure the interfacial energy between crystal and solution for NaCl–water system without assuming a fixed value of the pre-exponential factor. This suggests that the commonly accepted experimental value of  $A$  and  $\gamma$  for NaCl crystallization may need to be re-examined. Given that the current theoretical simulations generally

overestimate the experimental nucleation rates [Fig. 3], our findings can serve as additional experimental data for comparison, leading to new insights that could bridge the gap between theory and experiments.

Overall, we highlight that these interesting finite-size effects are clearly observable in our microfluidic experiments, which would not be observed in bulk solution experiments. The data treatment of our experiments with the CNT model allows us to have a better understanding of nucleation, providing kinetic and thermodynamic information on the system NaCl/water.

#### IV. CONCLUSION

To summarize, we report a stochastic approach to extract the nucleation kinetic parameters from the induction time distribution of evaporating sessile microdroplets using NaCl–water as a model system. We showed that by combining a modified Poisson distribution analysis together with an accurate evaporation model, one could obtain reliable nucleation kinetic parameters (both kinetic and thermodynamic). Our results also reveal the competition between the nucleation-enhancing heterogeneous mechanism and the nucleation-inhibiting confinement effects. However, to fully elucidate the underlying mechanisms, it would be interesting to investigate a wider range of droplet sizes together with finer control of evaporation rate, allowing the study of the impact of the rate of change of supersaturation ratio. To investigate quantitatively the impact of thermodynamic confinement, modeling the distributions of the pre-critical clusters would be essential. The use of non-classical nucleation theories can also be explored.

Given the numerous simulation studies on NaCl nucleation,<sup>8,10–14</sup> our experimental nucleation parameters based on the stochastic approach presented here can serve as additional data points for comparison with theoretical predictions. Moreover, our experimental approach and data-treatment protocol can also be extended to study the nucleation of other salts, biological, and pharmaceutical crystals of interest.

## SUPPLEMENTARY MATERIAL

See supplementary material for details of the Classical Nucleation Theory for ionic systems; details of the modified Poisson distribution function; details of ionic activity coefficient vs supersaturation ratio; details of evaporation model; details of data processing and curve fitting method; details of the effect of solubility on thermodynamic confinement; and details of statistical analysis of  $\tau$ -distributions.

## ACKNOWLEDGMENTS

RC acknowledges the financial support of the Vidyasirimedhi Institute of Science and Technology (VISTEC) and the Eiffel Excellence Scholarship (N° Grant No. P744524E) granted by the French Government. NL was supported by the French National Research Agency (Grant No. ANR-16-CONV-0001) and the Excellence Initiative of Aix-Marseille University–A\* MIDEEX.

## AUTHOR DECLARATIONS

### Conflict of Interest

The authors have no conflicts to disclose.

## Author Contributions

**Ruel Cedeno:** Formal analysis (equal); Methodology (equal); Writing – review & editing (equal). **Romain Grossier:** Conceptualization (equal); Formal analysis (equal); Supervision (equal); Writing – review & editing (equal). **Nadine Candoni:** Conceptualization (equal); Supervision (equal). **Nicolas Levernier:** Conceptualization (supporting). **Adrian E. Flood:** Supervision (equal); Writing – original draft (equal). **Stéphane Veesler:** Conceptualization (equal); Supervision (equal); Writing – original draft (equal).

## DATA AVAILABILITY

The data that support the findings of this study are available from the corresponding authors upon reasonable request.

## REFERENCES

- J. Lee, J. Yang, S. G. Kwon, and T. Hyeon, *Nat. Rev. Mater.* **1**(8), 16034 (2016).
- J. H. Um, A. Jin, X. Huang, J. Seok, S. S. Park, J. Moon, M. Kim, S. H. Kim, H. S. Kim, S.-P. Cho, H. D. Abruña, and S.-H. Yu, *Energy Environ. Sci.* **15** (4), 1493–1502 (2022).
- R. D. Davis, S. Lance, J. A. Gordon, S. B. Ushijima, and M. A. Tolbert, *Proc. Natl. Acad. Sci. U. S. A.* **112**(52), 15815 (2015).
- J. Desarnaud, H. Derluyn, J. Carmeliet, D. Bonn, and N. Shahidzadeh, *J. Phys. Chem. Lett.* **5**(5), 890–895 (2014).
- G. S. Frankel, J. D. Vienna, J. Lian, X. Guo, S. Gin, S. H. Kim, J. Du, J. V. Ryan, J. Wang, W. Windl, C. D. Taylor, and J. R. Scully, *Chem. Rev.* **121**(20), 12327–12383 (2021).
- E. M. Winkler and P. C. Singer, *Geol. Soc. Am. Bull.* **83**(11), 3509–3514 (1972).
- M. J. Qazi, R. W. Liefferink, S. J. Schlegel, E. H. G. Backus, D. Bonn, and N. Shahidzadeh, *Langmuir* **33**(17), 4260–4268 (2017).
- N. E. R. Zimmermann, B. Vorselaars, J. R. Espinosa, D. Quigley, W. R. Smith, E. Sanz, C. Vega, and B. Peters, *J. Chem. Phys.* **148**(22), 222838 (2018).
- K. E. Blow, D. Quigley, and G. C. Sosso, *J. Chem. Phys.* **155**(4), 040901 (2021).
- N. E. R. Zimmermann, B. Vorselaars, D. Quigley, and B. Peters, *J. Am. Chem. Soc.* **137**(41), 13352–13361 (2015).
- D. Zahn, *Phys. Rev. Lett.* **92**(4), 040801 (2004).
- R. Bahadur, L. M. Russell, and S. Alavi, *J. Phys. Chem. B* **111**(41), 11989–11996 (2007).
- G. Lanaro and G. N. Patey, *J. Phys. Chem. B* **120**(34), 9076–9087 (2016).
- H. Jiang, A. Haji-Akbari, P. G. Debenedetti, and A. Z. Panagiotopoulos, *J. Chem. Phys.* **148**(4), 044505 (2018).
- Y. Gao, L. E. Yu, and S. B. Chen, *J. Phys. Chem. A* **111**(42), 10660–10666 (2007).
- H.-S. Na, S. Arnold, and A. S. Myerson, *J. Cryst. Growth* **139**(1), 104–112 (1994).
- L.-T. Deck and M. Mazzotti, *Cryst. Growth Des.* **23**(2), 899–914 (2022).
- N. Candoni, Z. Hammadi, R. Grossier, M. Ildefonso, S. Zhang, R. Morin, and S. Veesler, in *Advances in Organic Crystal Chemistry: Comprehensive Reviews 2015*, edited by R. Tamura and M. Miyata (Springer, Japan, Tokyo, 2015), pp. 95–113.
- R. Grossier, Z. Hammadi, R. Morin, and S. Veesler, *Phys. Rev. Lett.* **107**(2), 025504 (2011).
- T. Nakamuro, M. Sakakibara, H. Nada, K. Harano, and E. Nakamura, *J. Am. Chem. Soc.* **143**(4), 1763–1767 (2021).
- R. Cedeno, R. Grossier, M. Lagaize, D. Nerini, N. Candoni, A. Flood, and S. Veesler, *Faraday Discuss.* **235**, 183–197 (2022).
- R. Cedeno, R. Grossier, V. Tishkova, N. Candoni, A. E. Flood, and S. Veesler, *Langmuir* **38**(31), 9686–9696 (2022).
- L. Goh, K. Chen, V. Bhamidi, G. He, N. C. S. Kee, P. J. A. Kenis, C. F. Zukoski III, and R. D. Braatz, *Cryst. Growth Des.* **10**(6), 2515–2521 (2010).
- X. Y. Liu, *Langmuir* **16**(18), 7337–7345 (2000).
- F. C. Meldrum and C. O’Shaughnessy, *Adv. Mater.* **32**(31), 2001068 (2020).
- R. Grossier and S. Veesler, *Cryst. Growth Des.* **9**(4), 1917–1922 (2009).
- O. A. Bempah and O. E. Hileman, Jr., *Can. J. Chem.* **51**(20), 3435–3442 (1973).
- R. Grossier, V. Tishkova, R. Morin, and S. Veesler, *AIP Adv.* **8**(7), 075324 (2018).
- B. Peters, *J. Cryst. Growth* **317**(1), 79–83 (2011).
- N. Shahidzadeh, M. F. L. Schut, J. Desarnaud, M. Prat, and D. Bonn, *Sci. Rep.* **5**(1), 10335 (2015).
- P. Koß, A. Statt, P. Virnau, and K. Binder, *Phys. Rev. E* **96**(4), 042609 (2017).
- M. W. Anderson, M. Bennett, R. Cedeno, H. Cölfen, S. J. Cox, A. J. Cruz-Cabeza, J. J. De Yoreo, R. Drummond-Brydson, M. K. Dudek, K. A. Fichthorn, A. R. Finney, I. Ford, J. M. Galloway, D. Gebauer, R. Grossier, J. H. Harding, A. Hare, D. Horváth, L. Hunter, J. Kim, Y. Kimura, C. E. A. Kirschhock, A. A. Kiselev, W. Kras, C. Kuttner, A. Y. Lee, Z. Liao, L. Maini, S. O. Nilsson Lill, N. Pellens, S. L. Price, I. B. Rietveld, J. D. Rimer, K. J. Roberts, J. Rogal, M. Salvalaglio, I. Sandei, G. Schuszter, J. Sefcik, W. Sun, J. H. ter Horst, M. Ukrainczyk, A. E. S. Van Driessche, S. Veesler, P. G. Vekilov, V. Verma, T. Whale, H. P. Wheatcroft, and J. Zeglinski, *Faraday Discuss.* **235**, 219–272 (2022).

- <sup>33</sup>S. Karthika, T. K. Radhakrishnan, and P. Kalaichelvi, *Cryst. Growth Des.* **16**(11), 6663 (2016).
- <sup>34</sup>M. A. Durán-Olivencia, P. Yatsyshin, S. Kalliadasis, and J. F. Lutsko, *New J. Phys.* **20**(8), 083019 (2018).
- <sup>35</sup>H. Hwang, Y. C. Cho, S. Lee, Y.-H. Lee, S. Kim, Y. Kim, W. Jo, P. Duchstein, D. Zahn, and G. W. Lee, *Chem. Sci.* **12**(1), 179–187 (2021).
- <sup>36</sup>C. P. Lamas, J. R. Espinosa, M. M. Conde, J. Ramírez, P. Montero de Hijes, E. G. Noya, C. Vega, and E. Sanz, *Phys. Chem. Chem. Phys.* **23**(47), 26843–26852 (2021).
- <sup>37</sup>A. P. Olsen, R. C. Flagan, and J. A. Kornfield, *Rev. Sci. Instrum.* **77**(7), 073901 (2006).
- <sup>38</sup>A. Naillon, P. Joseph, and M. Prat, *J. Cryst. Growth* **463**, 201–210 (2017).



## Supplementary Material for:

# CNT effective interfacial energy and pre-exponential kinetic factor from measured NaCl crystal nucleation time distributions in contracting microdroplets

Ruel Cedeno<sup>1,2</sup>, Romain Grossier<sup>1</sup>, Nadine Candoni<sup>1</sup>, Nicolas Levernier<sup>3</sup>, Adrian Flood<sup>2\*</sup>, Stéphane Veessler<sup>1\*</sup>

<sup>1</sup>CNRS, Aix-Marseille University, CINaM (Centre Interdisciplinaire de Nanosciences de Marseille), Campus de Luminy, Case 913, F-13288 Marseille Cedex 09, France

<sup>2</sup>Department of Chemical and Biomolecular Engineering, School of Energy Science and Engineering, Vidyasirimedhi Institute of Science and Technology, Rayong 21210, Thailand

<sup>3</sup>INMED, INSERM, Aix Marseille Univ, France, Turing Centre for Living systems, Marseille, France ; CPT : Aix Marseille Univ, Université de Toulon, CNRS, CPT (UMR 7332), Turing Centre for Living systems, Marseille, France

## S1. Classical Nucleation Theory for Ionic Systems

Classical Nucleation theory expresses the primary nucleation rate  $J$  as the product of the pre-exponential factor  $A$  and an exponential factor containing the free energy cost of forming a critical nucleus  $\Delta G^*$  and thermal energy  $k_b T$ .

$$J = A \exp\left(-\frac{\Delta G^*}{k_b T}\right) \quad (S1)$$

An important difference between the treatment of ionic systems and molecular systems is in the expression of chemical potential difference between solid and liquid.<sup>1</sup> For ionic systems, it is a function of the number of ions forming one formula unit  $v$  (2 for NaCl), and the mean ionic activity coefficient of the solute  $\gamma_{\pm}$ . These lead to the following expression for  $\Delta G^*$

$$\Delta G^* = \frac{4}{3} \pi \gamma (R_c)^2 \quad \text{with} \quad R_c = \frac{2\gamma}{v k T \rho_s \ln\left(\frac{\gamma_{\pm}}{\gamma_{\pm 0}} S\right)} \quad (S2)$$

with interfacial energy  $\gamma$  between crystal and solution, critical radius  $R_c$ , number density of formula units in the solid  $\rho_s$  ( $2.27 \times 10^{28} \text{ m}^{-3}$  for NaCl), and  $S$  is the supersaturation ratio ( $c/c_{\text{sat}}$ )<sup>1</sup>.

## S2. Modified Poisson Distribution Function

In the stochastic view of nucleation, the probability distribution of the nucleation times must be analyzed. In the context of microdroplets, it is normally assumed that the time it takes for a nucleus to grow to detectable size is negligible<sup>2</sup>.

Thus, for constant supersaturation experiments, the cumulative probability of obtaining a droplet with at least one nucleus after time  $t$  is a function of nucleation rate  $J$  and droplet volume  $V$  given as

$$P(t) = 1 - \exp(-JVt) \quad (S3)$$

In the case of evaporating droplet, both the supersaturation and the volume vary with time. As suggested by Goh et. al.,<sup>2</sup> the cumulative probability distribution function becomes

$$P(t) = 1 - \exp \left[ - \int_{t_{\text{sat}}}^{t_{\text{nuc}}} J(t)V(t)dt \right] \quad (S4)$$

In equation (S4),  $J(t)$  can be expressed as a function of supersaturation  $S(t)$  by combining with equations (S1) through (S2) . The value of  $V(t)$  and  $S(t)$  was obtained from an evaporation model (section S4).

### S3. Ionic Activity Coefficient vs Supersaturation Ratio

The ionic activity coefficient is necessary to calculate the chemical potential from concentration. To obtain the activity coefficient as a function of supersaturation ratio, we employed the experimental data of Na et al.<sup>3</sup> We then used an empirical function (logistic) to fit the data.

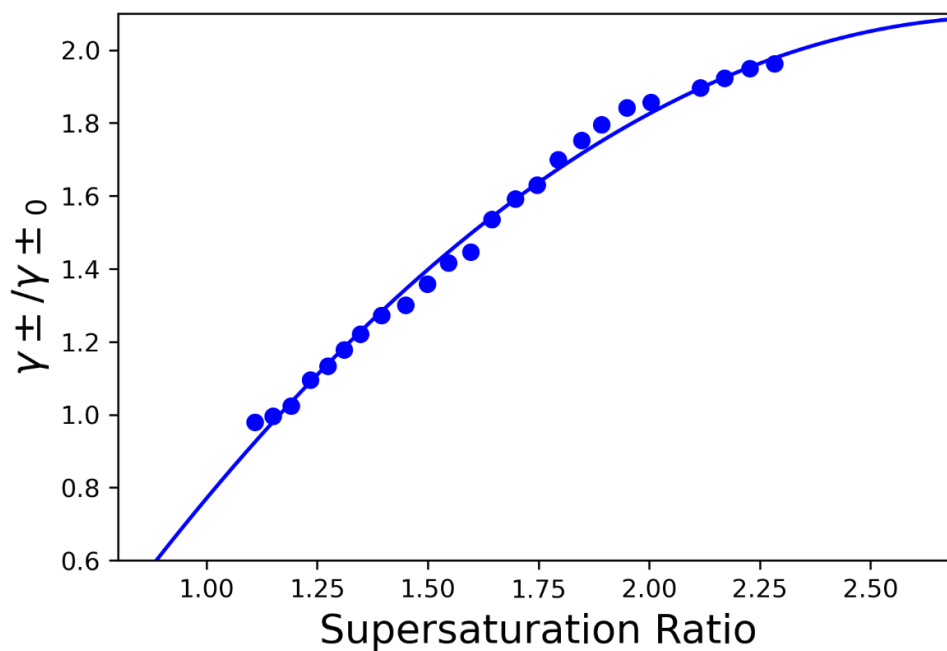


**Figure S1.** Ratio of ionic activity coefficients  $\gamma_{\pm}/\gamma_{\pm 0}$  based on the experimental data of Na et al.<sup>3</sup> The data is fitted with a general logistic function  $y = a/(1+\exp(-b(x-c)))$  resulting in  $a = 2.1889$ ,  $b=2.147$ ,  $c=1.241$  with  $R^2 = 0.995$ .

## S4. Evaporation Model

### S4.1. Evolution of Microdroplet Volume , Supersaturation Ratio, and Evaporate Rates

To determine the supersaturation ratio as a function of nucleation time, we used an evaporation model tailored for our specific system.<sup>4</sup> The evolution of volume and supersaturation with time are plotted as follows. As expected, smaller droplets evaporate faster due to higher surface area to volume ratio. For comparison, the prediction of a simple linear model (constant evaporation rate) is shown (dotted line).

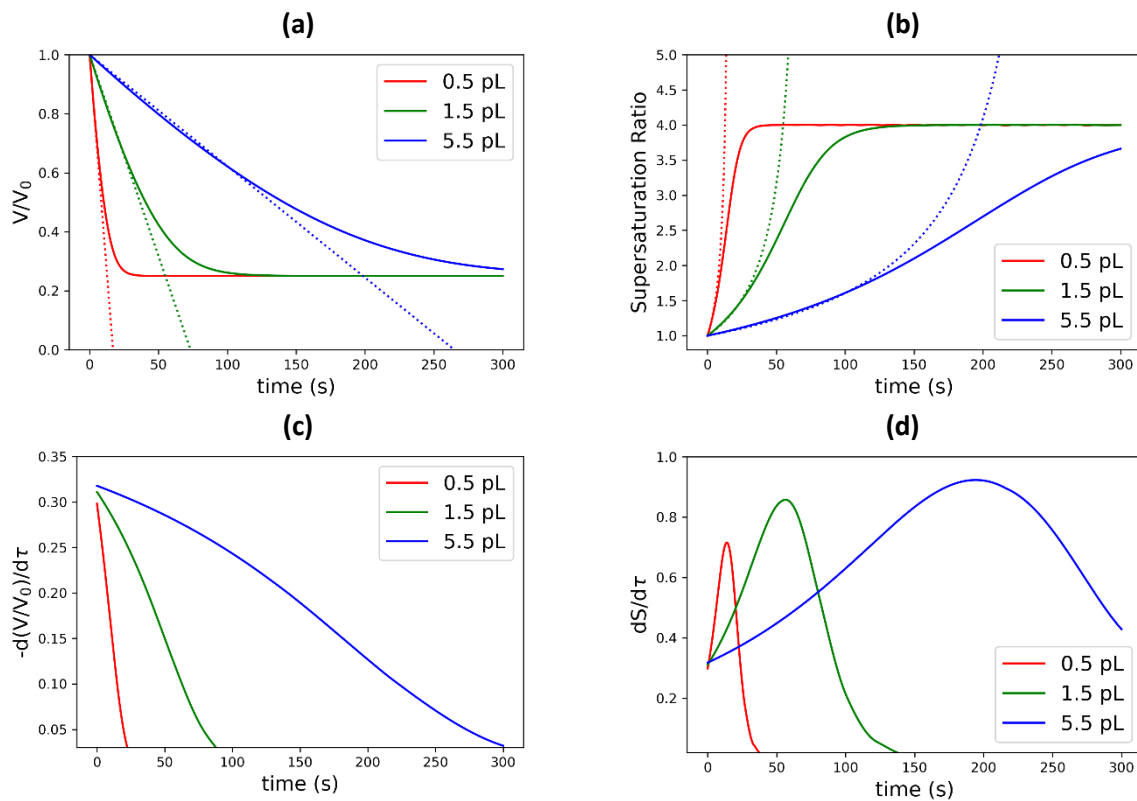


**Figure S2.** (a) Time evolution of normalized volume ( $V/V_0$ ) and (b) supersaturation ratio, calculated using our tailor-made evaporation model (solid line)<sup>4</sup> and a simple linear model (dotted line). (c) Dimensionless evaporation rate  $-d(V/V_0)/d\tau$  (d) Dimensionless rate of change of supersaturation  $dS/d\tau$  ratio.

## S4.2 Comparison with constant evaporation rate model

The use of simple linear model has been shown to overestimate the supersaturation ratio at nucleation particularly at the later stages of the evaporation process where the changes in water activity due to the presence of salt becomes significant (demonstrated in our previous work).<sup>4</sup> Here, we show the survival probability plot comparing our evaporation model against that of the simple model. The linear model predicts a maximum  $S$  of more than 4 which is highly unlikely for the NaCl-water system.

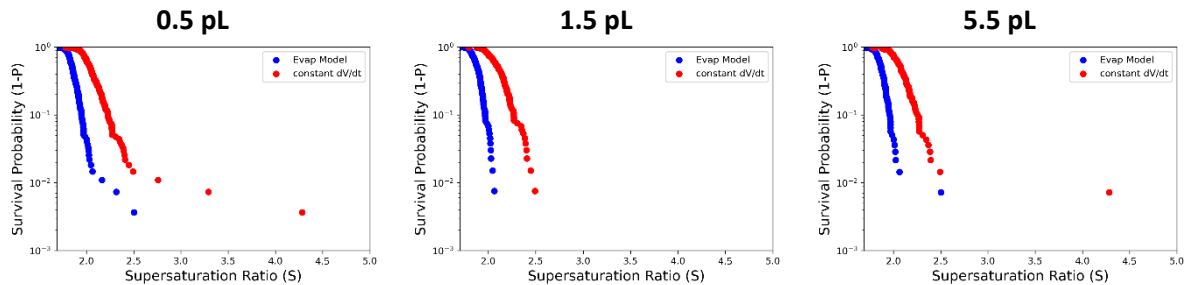


**Figure S3.** Survival probability plot of supersaturation ratios at nucleation calculated using a system-specific evaporation model (blue) compared against that of a simple linear model (red).

## S4.3 Homogeneity of Concentration in Microdroplet

Peclet number  $Pe$  is a dimensionless parameter which correlates the relative importance of convective and diffusive transport phenomena.

$$Pe = \frac{2R\kappa}{D_i}$$

where  $\kappa$  is the evaporation flux (volume loss  $dV/dt$  per unit area  $A$ ),  $R$  is the droplet radius and  $D_i$  is the diffusion coefficient of the solute in the droplet (in this case NaCl ions in water). Generally,  $Pe \ll 1$  denotes a homogeneous droplet concentration as the diffusion dominates over convection (i.e., no accumulation of solutes in the droplet interface or contact line).

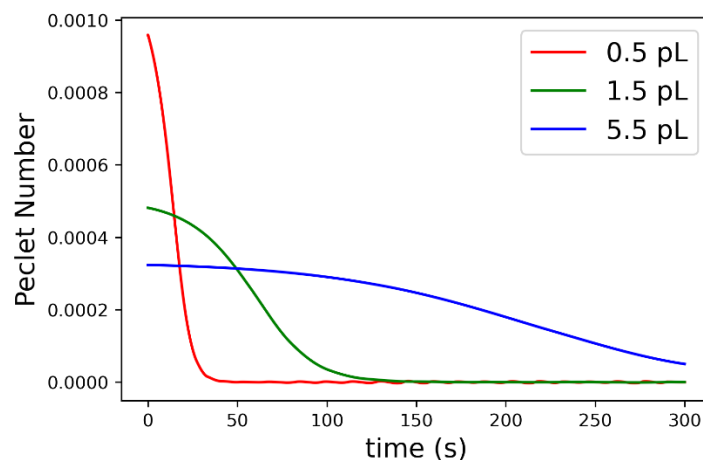


**Figure S4.** Peclet number as a function of time.

#### S4.4. Sensitivity with respect to the empirical parameter of the evaporation model

The evaporation model<sup>4</sup> contains an empirical parameter  $n_x$  which corresponds to the effective number of neighboring droplets that contribute to the local relative humidity. This parameter  $n_x$  was adjusted for each droplet size such that the experimental matching time is accurately reproduced. Here, we show that the resulting distribution of  $S_N$  (supersaturation at nucleation) is not sensitive to this empirical parameter. Therefore, the estimated CNT parameters are not sensitive to the adjustment of  $n_x$ .

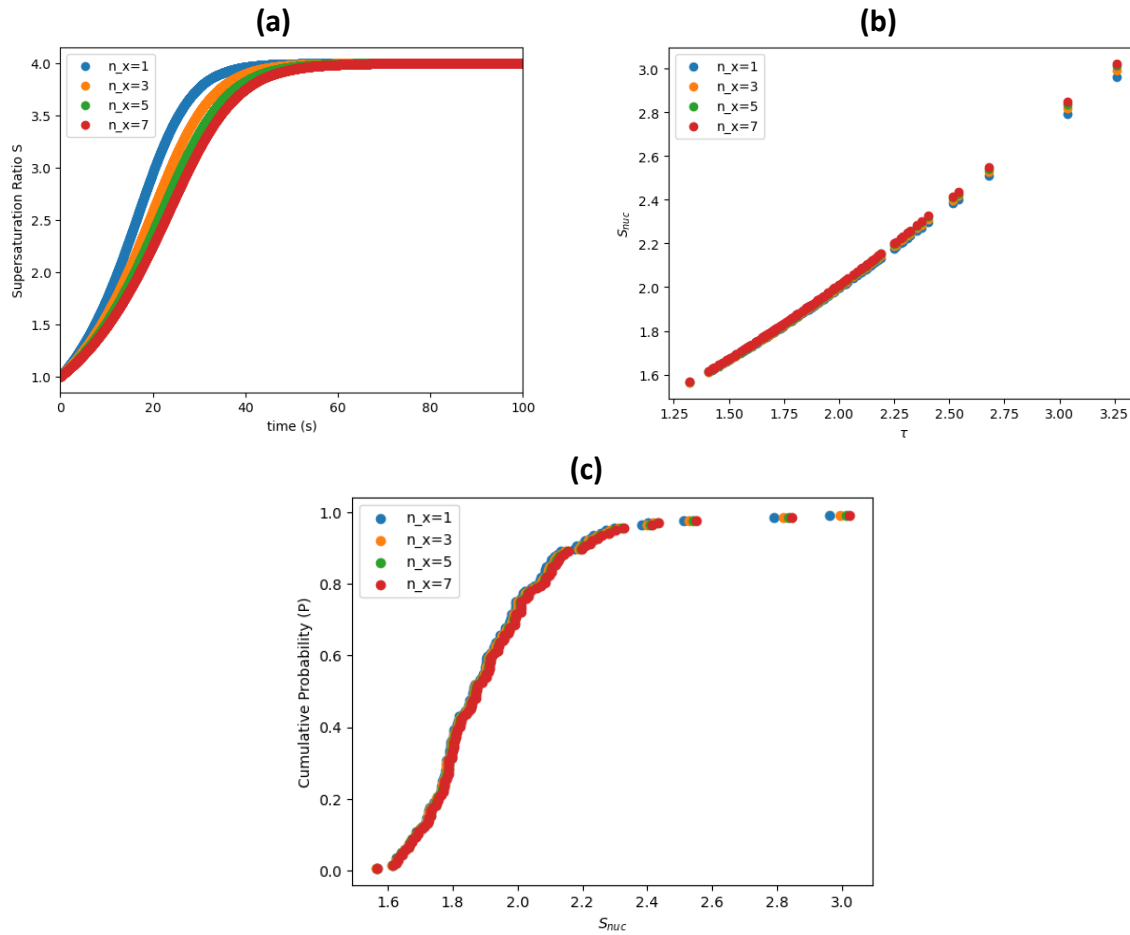


**Figure S5.** Impact of different values of empirical parameter  $n_x$  on (a) Supersaturation vs time (b) supersaturation ratio  $S_{Nuc}$  vs normalized time  $\tau$  (c) probability distribution of  $S_{Nuc}$

## S5. Data Processing and Curve fitting method

From the microscopy images, we analyzed the standard deviation of the gray-level pixels  $\sigma$  of the region surrounding a microdroplet. The plot of  $\sigma$  vs time allows the extraction of characteristic times  $t_{sat}$  (saturation time),  $t_{match}$  (matching time), and  $t_{nuc}$  (nucleation time). From these characteristic times, we can calculate a dimensionless nucleation time

$$\tau = \frac{t_{nuc} - t_{sat}}{t_{match} - t_{sat}}$$

More details of this procedure (as well as the statistical treatment of outliers) is in Ref.<sup>5</sup>

To obtain the supersaturation ratio  $S$  at any  $\tau$ , we employed a tailored evaporation model.<sup>4</sup>

The evaporation model contains an empirical parameter  $n_x$  which can be adjusted such that the theoretical matching time  $\tilde{t}_{match}$  reproduces the experimental median matching time  $\bar{t}_{match}$  after saturation (results are not sensitive to  $n_x$  adjustments as shown in S4.2).

The evaporation model then allows the calculation of supersaturation ratio  $S(t)$  and volume  $V(t)$  as a function of time  $t$ . Note that the time variable  $t$  in the evaporation model is referenced with respect to  $t_{sat}$  (i.e.,  $t = 0$  at  $S = 1$ ). Consequently, the correspondence between the  $t$ -scale and  $\tau$ -scale is given by

$$\tau = \frac{t}{\tilde{t}_{match}}$$

This correspondence allows us to calculate  $S(t)$  and  $V(t)$  at any given  $\tau$  which are needed in the evaluation of the inhomogeneous Poisson equation coupled with classical nucleation theory as follows:

$$P(t) = 1 - \exp \left[ - \int_{t_{sat}}^{t_{nuc}} J(t)V(t)dt \right]$$

where

$$J(t) = A \exp \left[ - \frac{16\pi}{3} \frac{\gamma_{eff}^3}{\rho_s^2 (k_b T)^3 \ln^2 \frac{\gamma_{\pm} S(t)}{\gamma_{\pm 0}}} \right]$$

Note that  $P(t)$  is coupled simultaneously with  $J(t)$  to find the values of  $A$  and  $\gamma_{eff}$  that minimize the squared residuals between the experimental and modeled  $P(t)$ , similar to that of Goh et al<sup>2</sup>. This means that the nucleation rate  $J$  is accessible after the fitting. For the curve fitting, we used the least-squares method 'leastsq' as implemented in the LMFIT<sup>6</sup> module.

## S6. Effect of Solubility on Thermodynamic Confinement

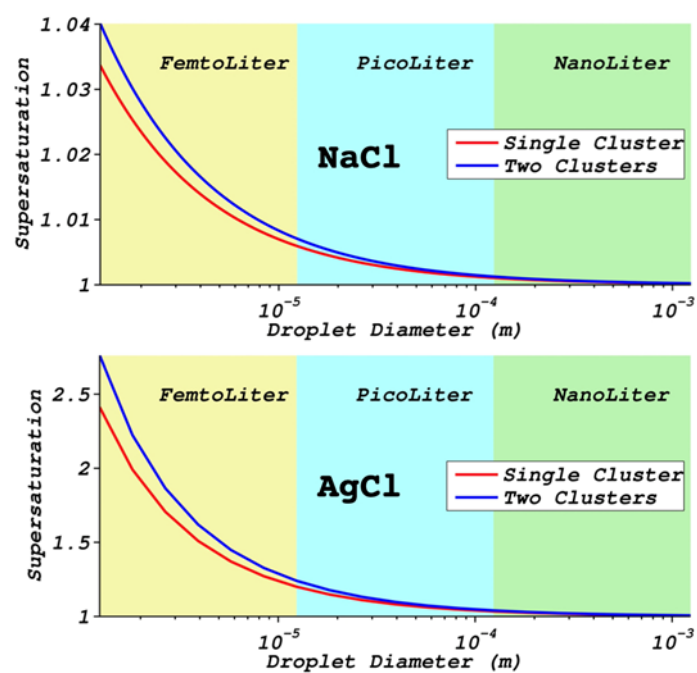


**Figure S6.** Effective supersaturation upon cluster formation as a function of droplet diameter for model compounds NaCl (high solubility) and AgCl (low solubility). Due to the lower solubility of AgCl, confinement-induced depletion of supersaturation needed to form a single critical-cluster is more dramatic effect in AgCl than NaCl. (Adapted from Ref<sup>7</sup>).



## S7. Statistical Analysis of $\tau$ -Distributions

### S7.1 Reproducibility of Experimental Sets

To assess the reproducibility of the  $\tau$ -distributions, we analyzed the cumulative probability plots of different experimental sets. Each set corresponds to a group of microdroplets located on the same “line” in the oil bath at a distinct cycle number (i.e. 3 lines with 2 cycles would result in 6 sets). As shown in our previous work, each set can be regarded as “independent” (i.e. negligible patterning and memory effects).<sup>5</sup> We applied a statistical treatment for detecting and eliminating outliers ( $k$ -sample Anderson-Darling test) demonstrated in our previous work.<sup>5</sup> The test employs a null hypothesis that the given distributions are statistically identical. Upon eliminating outliers, the results reveal that at 95% confidence level, there is no significant difference between the distribution of each set (i.e.  $p$ -values  $> 0.05$ ), thus they can be aggregated to form a larger distribution containing 131, 337, and 187 microdroplets for 0.5 pL, 1.5 pL, and 5.5 pL respectively.

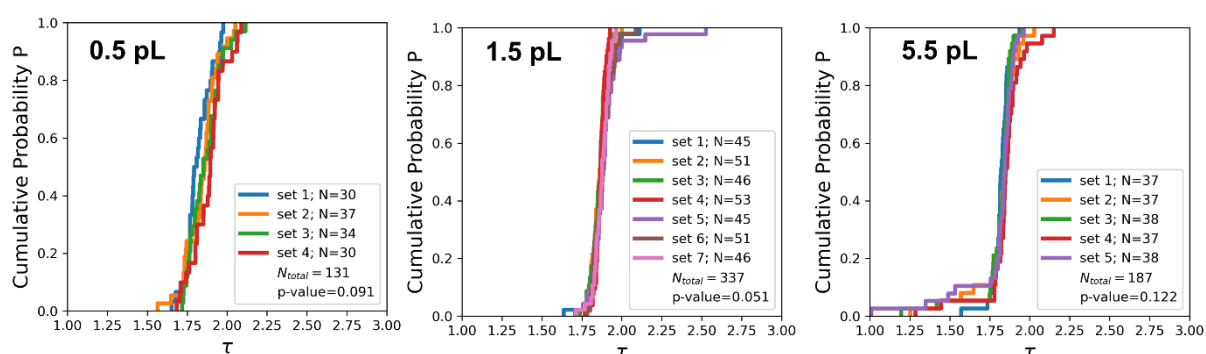


**Figure S7.** Cumulative probability of dimensionless nucleation time  $\tau$  of different experimental sets for each microdroplet volume. The  $p$ -values  $> 0.05$  suggest no significant difference between each experimental set within the same volume.

### S7.2 Comparing $\tau$ -Distributions from different volumes

To determine whether the observed difference in  $\tau$ -distributions obtained from different volumes is statistically significant, we again employed the  $k$ -sample Anderson-Darling test (null hypothesis: the given distributions are statistically identical). This resulted in a  $p$ -value of less than 0.001 (null hypothesis is rejected). Therefore, the three distributions are statistically different. Moreover, all pairwise comparisons (i.e., 0.5 vs 1.5 pL, 1.5 vs 5.5 pL, 0.5 vs 5.5 pL) also resulted in  $p$ -values  $< 0.001$ .

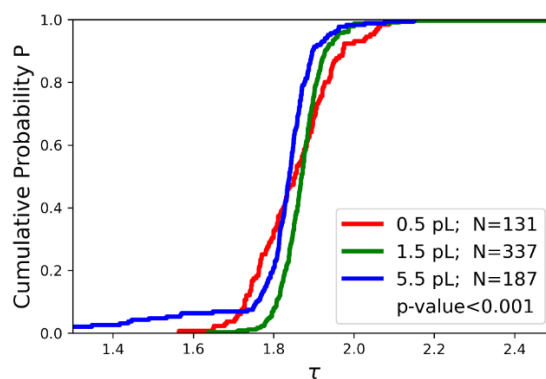


**Figure S8.** Cumulative probability of aggregated dimensionless nucleation time  $\tau$  for each microdroplet volume. The  $p$ -value  $< 0.001$  suggests a highly significant difference between the three distributions.

## References

1. J. Desarnaud, H. Derluyn, J. Carmeliet, D. Bonn and N. Shahidzadeh, *The Journal of Physical Chemistry Letters* **5** (5), 890-895 (2014).
2. L. Goh, K. Chen, V. Bhamidi, G. He, N. C. Kee, P. J. Kenis, C. F. Zukoski, 3rd and R. D. Braatz, *Cryst. Growth Des.* **10** (6), 2515-2521 (2010).
3. H.-S. Na, S. Arnold and A. S. Myerson, *J. Cryst. Growth* **139** (1), 104-112 (1994).
4. R. Cedeno, R. Grossier, V. Tishkova, N. Candoni, A. E. Flood and S. Veessler, *Langmuir* **38** (31), 9686-9696 (2022).
5. R. Cedeno, R. Grossier, M. Lagaize, D. Nerini, N. Candoni, A. Flood and S. Veessler, *Faraday Discuss.* **235** (0), 183-197 (2022).
6. M. Newville, T. Stensitzki, D. B. Allen and A. Ingargiola, Zenodo (2014).
7. R. Grossier and S. Veessler, *Crystal Growth & Design* **9** (4), 1917-1922 (2009).